CrossMark

ORIGINAL ARTICLE

Observations of quiet-time moderate midlatitude L-band scintillation in association with plasma bubbles

S. Vadakke Veettil[1] · H. Haralambous[2] · M. Aquino[1]

Abstract Observations of moderate night time amplitude scintillation on the GPS L1C/A signal were recorded at the midlatitude station of Nicosia, corresponding geographic latitude and longitude of 35.18°N and 33.38°E respectively, on a geomagnetically quiet day. The variations of slant total electron content (STEC) and amplitude scintillation index (S4) on the night of June 12, 2014, indicate the presence of electron density depletions accompanying scintillation occurrence. The estimated apparent horizontal drift velocity and propagation direction of the plasma depletions are consistent with those observed for the equatorial plasma bubbles, thus suggesting that the moderate amplitude L-band scintillation observed over Nicosia may be associated with the extension of such plasma bubbles. The L-band scintillation occurrence was concurrent with the observations of range spread F on the ionograms recorded by the digisonde at Nicosia. The height–time–intensity plot generated using the ionogram data also showed features which can be attributed to off-angle reflections from electron density depletions, thus corroborating the STEC observations. This observation suggests that the midlatitude ionosphere is more active even during geomagnetically quiet days than previously thought and that further studies are necessary. This is particularly relevant for the GNSS user community and related applications.

Introduction

Scintillation of transionospheric radio signals is a consequence of electron density irregularities that may occur within the ionosphere and is characterized by rapid fluctuations in the amplitude and phase of these signals when they pass through the ionosphere (Kintner et al. 2001). The occurrence of scintillation shows considerable spatial and temporal variability, with dependence on local time, season, latitude, solar and geomagnetic activity. The global morphology of ionospheric L-band scintillation occurrence is presented in Basu et al. (2002), which reports that scintillation occurrence is strong over the equatorial latitudes extending from 20°N to 20°S geomagnetic latitudes, moderate to strong over the high latitudes extending from 65° to 90° geomagnetic latitudes and almost absent over the midlatitudes. The midlatitude ionosphere is generally considered to lack the necessary processes required to generate the irregularities causing scintillation and hence is regarded as a less scintillation active region. However, Maruyama (1990) has shown that over the midlatitudes, the ExB instability can be excited when a significantly strong eastward electric field is present, giving rise to intense irregularities and L-band scintillation.

A number of midlatitude scintillation studies have been carried out mainly using the VHF radio transmissions from geostationary satellites, as lower frequencies are more severely affected (Kersley et al. 1980; Hajkowicz and Minakoshi 2003). Using a 5-year data set from 150 MHz radio transmissions, Hajkowicz (1994) reported that

✉ S. Vadakke Veettil
v.sreeja@gmail.com

1   Nottingham Geospatial Institute, University of Nottingham, Triumph Road, Nottingham NG7 2TU, UK

2   Frederick University, Nicosia, Cyprus

🗫 Springer

localized midlatitude scintillation patches frequently occur during sunspot minimum, in association with the occurrence of midlatitude spread F. The observations of L-band scintillation at midlatitudes are mostly reported during severe geomagnetic storms (Ogawa and Kumagai 1985; Bust et al. 1997; Ma and Maruyama 2006) and during the equatorward movement of the ionospheric trough along with a storm time-enhanced density (SED) (Ledvina et al. 2002). Using the data from a geostationary satellite over Japan, Fujita et al. (1982) reported that the scintillation activity at 1.7 GHz is enhanced at night in June. Otsuka et al. (2006) carried out a statistical study on the latitudinal dependence of the irregularity characteristics over Japan by using total electron content (TEC) data obtained from the Global Positioning System (GPS) network in Japan during 2000. Their study revealed that at the midlatitudes, i.e., between 29 and 38°N, scintillation occurrence is highest during summer nighttime. A climatological study on the midlatitude (50–51°N geographic latitude) ionospheric quiet time disturbances based on 10 years of GPS data in Belgium revealed that the occurrence of summer night time disturbances is lower than that of their winter day time counterparts (Wautelet and Warnant 2014). The results from this study showed that the winter day time disturbances correspond to the classical medium scale traveling ionospheric disturbances (MSTIDs), exhibit properties matching the results reported in the literature (Tsugawa et al. 2007), whereas the summer night time disturbances correspond to non-classical MSTIDs of electrical origin. The origin of these two types of disturbances were further investigated in Wautelet and Warnant (2015), which showed that summer night time disturbances were related to the spread F phenomenon, linked to the appearance of sporadic E (Es) layers. In the United Kingdom (UK), Aquino et al. (2005) reported on the occurrence of GPS L1 phase scintillation recorded by the GPS NovAtel GSV4004B scintillation monitor receiver at the midlatitude station of Nottingham, corresponding geographic latitude and longitude of 52.95°N and 1.18°W, during the severe geomagnetic storm of November 6, 2001. They also reported on strong correlation between high levels of phase scintillation and positioning accuracy degradation at the same station during the Halloween storm of October 2003.

The observation of moderate amplitude scintillation on the GPS L1C/A signal recorded by a Septentrio PolaRxS receiver on a geomagnetically quiet day at the midlatitude station of Nicosia in Cyprus, is presented and discussed. The geographic latitude and longitude of Nicosia are 35.14°N and 33.48°E, respectively, and the corresponding geomagnetic latitude is 31.79°N. The next section describes the data and the method of analysis. The results and discussions are then presented in the subsequent section. Finally, the conclusions are presented in last section.

Data and methodology

A Septentrio PolaRxS GNSS receiver (Septentrio PolaRxS application manual 2010) was deployed in Nicosia under the UK Engineering and Physical Sciences Research Council (EPSRC) funded "Polaris" project (http://www.bath.ac.uk/elec-eng/polaris/) and has been routinely collecting ionospheric scintillation data since December 2011. This study is based on the analysis of one-minute scintillation indices, namely S4 and σ_φ, recorded on the GPS L1C/A signal during June 11–13, 2014. The amplitude scintillation index, S4, is the standard deviation of the received signal power normalized by its mean value and the phase scintillation index, σ_φ, is the standard deviation of the detrended carrier phase computed over 60 s, using a filter of 0.1 Hz cutoff (Van Dierendonck et al. 1993). Also, the S4 recorded on the L1 frequency by the EGNOS (European Geostationary Navigation Overlay Service) satellites is used. A satellite elevation angle cutoff of 20° is applied in order to reduce the impact of non-scintillation-related errors, e.g., induced by multipath. In order to investigate the presence of electron density gradients leading to the occurrence of scintillation, the Slant TEC (STEC) values recorded by the receiver at every minute interval are used to estimate the Rate of TEC (ROT), i.e., temporal change in STEC. The latitude and longitude of the ionospheric pierce point (IPP) for the different ray paths have been calculated assuming a thin single shell ionospheric model at an altitude of 350 km (Ciraolo and Spalla 1997).

In addition, data obtained from three GNSS receivers of the International GNSS Service (IGS) network is also used, in order to identify the presence of electron density irregularities. The approximate geographic and geomagnetic coordinates of these receivers are listed in Table 1. The data from the geodetic receiver at Nicosia are also used in the analyses to confirm the presence of irregularities recorded by the PolaRxS receiver. For the study, the data from station "Nama" represent the anomaly crest, while the data from "Haly" and "Nico" represent the locations beyond the anomaly crest. The RINEX observation files recorded by these receivers are processed to estimate the uncalibrated STEC values every 30 s for each ray path with elevation angle greater than 20°. The rate of TEC index (ROTI), defined as the standard deviation of ROT (Pi et al. 1997), is then computed over 5-min intervals to identify the presence of large-scale electron density irregularities.

The data acquired by the GPS Occultation Experiment (GOX) on the COSMIC (Constellation Observing System for Meteorology, Ionosphere, and Climate) satellite for the same period, downloaded from the COSMIC Data Acquisition and Analysis Center (CDAAC) web site (http://

Table 1 GNSS receiver type, geographic and geomagnetic coordinates of the station locations

Station name	Station code	Receiver type	Geographic latitude	Geographic longitude	Geomagnetic latitude
Namas	Nama	TRIMBLE NETRS	19.21142°N	42.04465°E	14.83°N
Halat Ammar	Haly	TRIMBLE NETRS	29.13887°N	36.09992°E	25.47°N
Nicosia	Nico	LEICA GR25	35.14098°N	33.39643°E	31.79°N

cosmic-io.cosmic.ucar.edu/cdaac/login/cosmic/), has also been used to confirm the L-band scintillation occurrence. This data are composed of "scnLv1″" files containing the 1 s S4 index calculated on the GPS L1C/A code (1.575 GHz), along with the signal-to-noise ratio on the L1C/A channel (caL1_SNR), produced for each observation and occultation of the GPS satellites observed by COSMIC (Carter et al. 2013). The values of S4max9s, defined as the 9 s average of the S4 values surrounding the time of maximum S4 (S4max) recorded in each occultation event, were extracted from these files. Along with the S4max9 s, the values of the alttp S4max, lcttp S4max, lattp S4max and lontp S4max were also extracted, which represent, respectively, the altitude, local time, latitude, and longitude of the occultation tangent point at the time the maximum S4 was measured.

To complement the data from the GNSS receivers, the ionograms, skymaps and drift velocities recorded at every 5 min by the DPS-4D digisonde operating at Nicosia are used. The Nicosia digisonde is a state-of-the-art ionosonde which performs optimal ionogram recordings based on the digisonde Precision Group Height Measurement (PGHM) technique (Reinisch et al. 2005) and ionospheric "drifts" using Doppler interferometry (Reinisch et al. 1998). The skymap is an interpretation view of the interferometry technique employed in digisonde to resolve individual echoes from the ionosphere ('sources') in terms of their position and velocity and therefore useful in providing direct confirmation for the presence of 'sources' in oblique directions.

The ionogram observations during June 11–13, 2014, are also analyzed based on the height–time–reflection intensity (HTI) methodology that is analogous to the technique producing range–time–intensity (RTI) radar displays within a given interval of time. The HTI technique is described in detail in Haldoupis et al. (2006) and in Lynn et al. (2013). In brief, this method considers an ionogram as a "snapshot" of reflected intensity as a function of height and ionosonde signal frequency, and uses a sequence of ionograms to compute, for a given frequency bin, an average HTI plot, i.e., a 3-D plot of reflected signal-to-noise ratio in dB as a function of height within a given time interval.

The characterization of the geomagnetic conditions during this period is performed using the planetary geomagnetic activity index Kp, the disturbance storm time

index Dst, and the auroral electrojet index AE, obtained from the World Data Center for Geomagnetism, Kyoto (http://wdc.kugi.kyoto-u.ac.jp/).

Results and discussions

Figure 1 shows the variations of the indices Kp (top), AE (middle) and Dst (bottom) during June 11–13, 2014. The 3-hourly Kp index is noticeably low during this period, reaching a maximum value of 2+ on June 11. The one-minute AE index is also generally low, and only few high values (>400 nT) are observed on that day. However, according to Prölss (1993), these are not large enough to trigger intense substorms. The hourly Dst index does not show high variability and the values fluctuate between +10 nT and −10 nT, suggesting that the disturbances are too
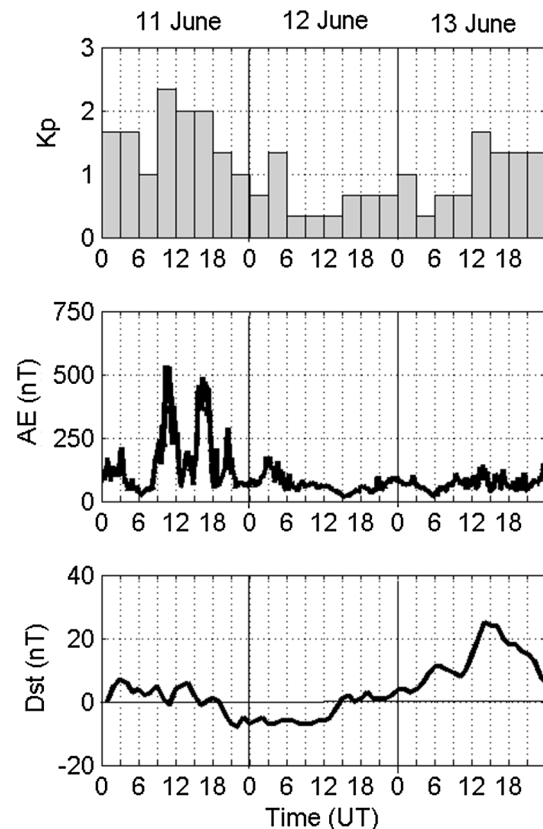

Fig. 1 Variation in the 3 hourly Kp (*top*), 1 min AE (*middle*) and 1 h Dst (*bottom*) indices during June 11–13, 2014

small to be considered as a geomagnetic storm. The Dst reaches values close to +30nT during the late evening hours on June 13. Altogether, these variations in the Kp, AE and Dst indices suggest that this period is characterized by quiet geomagnetic conditions.

GNSS measurements

The variations in the amplitude and phase scintillation indices, S4 and σ_φ, recorded by the PolaRxS receiver on the GPS L1C/A signal during June 11–13, 2014, over Nicosia are shown in Fig. 2. From this figure, moderate levels of amplitude scintillation, characterized by $0.3 < S_4 < 0.7$ (Alfonsi et al. 2011), can be observed during 20:00–24:00 UT on June 12. The corresponding σ_φ values are much lower, with maximum values around 0.3. For the GPS L1 frequency, the most effective spatial size of the electron density irregularities that causes amplitude scintillation is the first Fresnel scale, which corresponds to about 330–400 m when the altitude of the ionospheric F-region is about 300–400 km. Thus, the L-band moderate amplitude scintillation occurrence on the night of June 12, as observed in Fig. 2, indicates the presence of electron density irregularities at hundred-meter scale sizes.

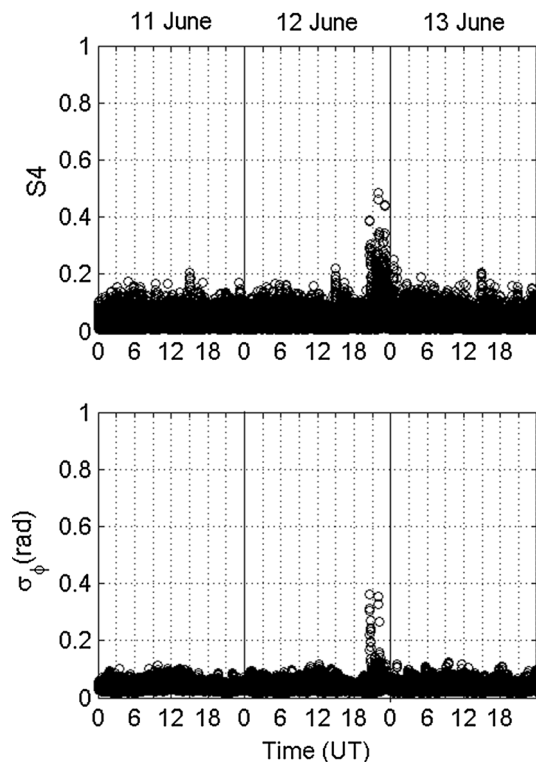In order to obtain an insight on the prevailing electron density gradients leading to the occurrence of scintillation, the variations in S4 (top) and ROT (bottom) are shown in Fig. 3 for 6 satellites in view during 20:00–24:00 UT on June 12. It can be observed that higher S4 values occur in correspondence with the steep electron density gradients indicated by the large variations in ROT. The high S4 values and varying ROT are mainly observed for the 4 satellites SV03, SV16, SV19, and SV27.

In order to investigate the geographic location of the electron density irregularities leading to the scintillation occurrence, Fig. 4 shows the S4 variations as a function of IPP latitude and longitude for individual satellite-receiver links during 20:00–24:00 UT. The location of the receiver at Nicosia is shown as a red circle in the figure. The satellite corresponding to each IPP trace is labeled as "SV" followed by the satellite number. The '+' sign indicates the initial location of the satellite. It can be observed from this figure that high S4 values are located within the latitudinal band of about 28–35°N and correspond only to satellites traveling southwards, namely SV03, SV16, SV19, and SV27, of the receiver location. Northward traveling satellites, i.e. SV22 and SV14, do not record any significant S4 values. On comparing the temporal and spatial variations in S4, as shown in Figs. 3 and 4 respectively, an eastward propagation of the irregularities can be observed.

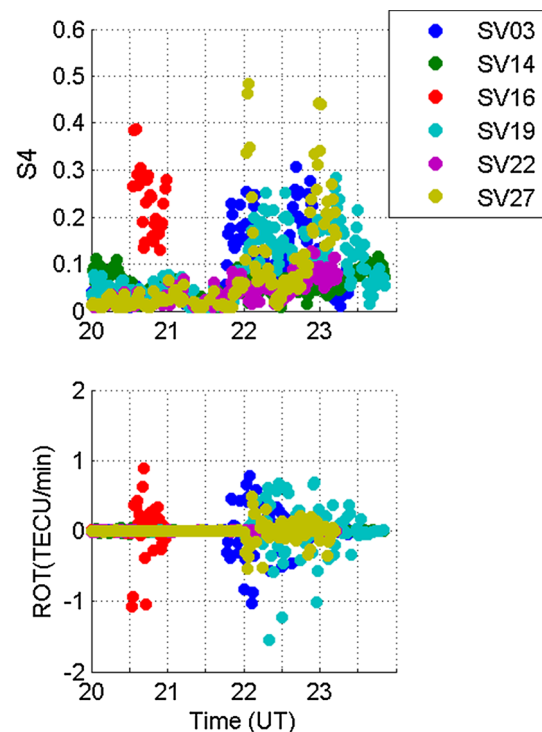To further ascertain the propagation direction and to determine the approximate zonal drift velocity of the

Fig. 2 Variation in the S4 and σ_φ indices recorded on the GPS L1C/A signal over Nicosia during June 11–13, 2014

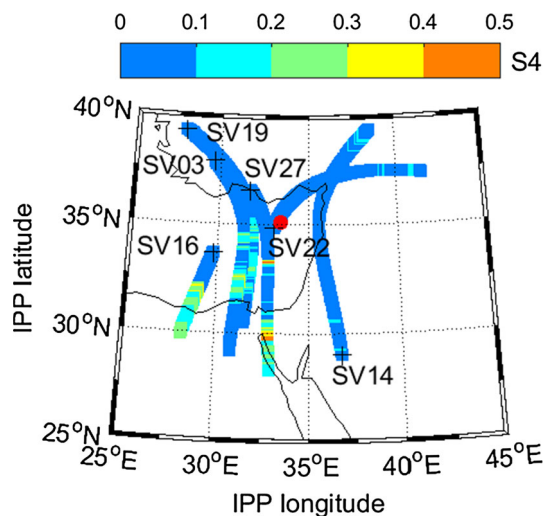**Fig. 3** S4 (top) and ROT (bottom) variations during 20:00–24:00 UT on June 12, 2014

Fig. 4 IPP tracks *shaded* with the S4 index as indicated in the *color bar*, for individual satellite-receiver links during 20:00–24:00 UT on June 12, 2014
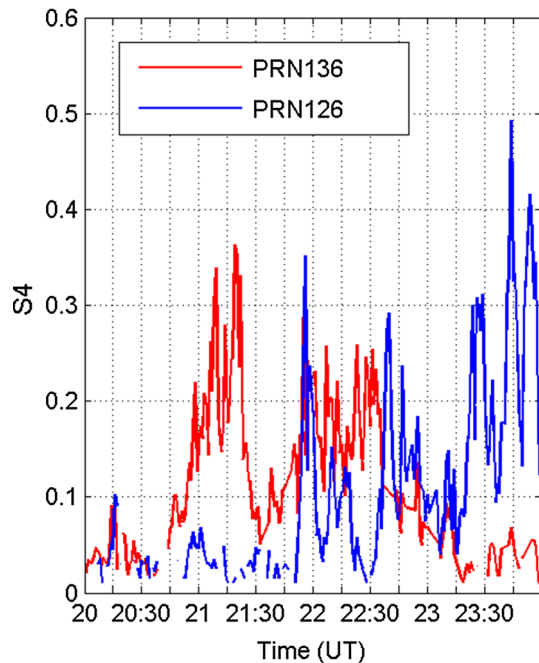

Fig. 5 S4 as observed by PRN136 (*red*) and PRN126 (*blue*) on June 12, 2014

irregularities, the temporal variations of S4 recorded on the L1 frequency by two EGNOS geostationary satellites, SES-5 and Inmarsat 4-F2, are shown in Fig. 5. The EGNOS SES-5, namely PRN136, is located at 5°E with a satellite elevation angle of 39°. The corresponding IPP latitude and longitude are 32.552°N and 30.957°E, respectively. The Inmarsat 4-F2, namely PRN126, is located at 25°E with a satellite elevation angle of 48°. The corresponding IPP latitude and longitude are 32.626°N and 32.743°E, respectively. This combination of two geostationary

satellites to estimate the zonal drift velocity has been used due to the absence of multiple zonally separated ground receivers, which would provide the ideal configuration (Ledvina et al. 2004). Though the S4 values along the two satellite-receiver links (PRN136 and PRN126) have been recorded by the same GNSS receiver at Nicosia, different regions of the ionosphere were probed due to the difference in the viewing geometry. The occurrence of scintillation on PRN136 (red line) precedes that on PRN126 (blue line), as the former is located west of the latter, clearly indicating the eastward propagation of the irregularities. As the two satellites are located along nearly the same IPP latitude, the longitudinal separation of the IPP points would correspond to the zonal separation. This distance along with the time lag between two nearby identifiable features, around 21:00 UT on PRN136 and around 22:00 UT on PRN126, yields an eastward component of the irregularity drift velocity as about 49 m/s.

Past research has shown that the apparent eastward zonal drift velocity of the plasma bubble peaks around 20:00–21:00 LT with average values of 150–200 m/s. After 22:00 LT, a gradual decrease in the zonal drift velocity from 100 to 200 m/s to below 50 m/s after local midnight is reported (Ji et al. 2015). The estimated drift velocity of about 49 m/s is observed around 22:00 UT, corresponding to the local midnight hours (LT = UT + 2.25 h) and thus matching the expected values.

An analysis of the scintillation data recorded by the COSMIC satellite on June 12 showed an S4max9 s value of 0.49 around 18:36 UT during an occultation event on GPS satellite SV25. Figure 6 shows the temporal variations in the 1 s S4 and L1 SNR. Fluctuations in the SNR along with high values of S4 can be clearly observed from this figure, indicating scintillation occurrence. The observed value of S4max is 0.787 at a tangent latitude and longitude of 26.1°N and 29.1°E, respectively. The corresponding tangent point altitude was 386 km, thus indicating the presence of electron density irregularities in the F-region (Carter et al. 2013). The scintillation observation from the COSMIC data further confirmed the presence of F-region irregularities on the night of June 12.

The observed scintillation on the night of June 12 can be attributed to an extension of the equatorial plasma bubbles or to locally generated irregularities. The Perkins instability is widely considered as the most likely mechanism for the generation of F-region irregularities over the midlatitudes and is known to cause oscillations in the TEC (Perkins 1973). On the other hand, the equatorial plasma bubbles can rise to high apex height and extend to higher latitudes by diffusing along the magnetic field lines (Huang et al. 2007). The presence of equatorial plasma bubbles can be identified from the
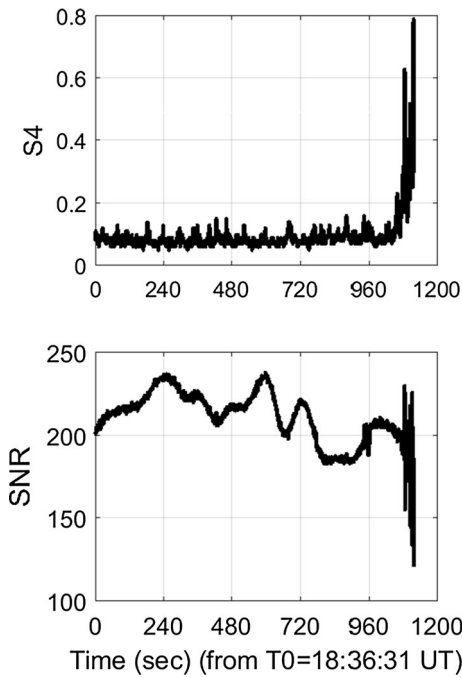
Fig. 6 Temporal profile of the 1 s S4 scintillation index (*top*) and SNR (*bottom*) of the LEO-GPS link on June 12, 2014

TEC variations as they manifest as depletions in TEC and characterized by sudden reduction in TEC followed by a recovery to the level of TEC preceding the reduction. Therefore, TEC variations will provide an invaluable insight on the possible source of the observed irregularities causing scintillation.

Figure 7 shows the variations in STEC (red) along with the S4 (black) for four satellite-receiver links, namely SV03, SV16, SV19 and SV27, at Nicosia, which recorded moderate scintillation. It can be observed from the figure that scintillation occurrence is coincident with TEC depletion and that these are observed on both the east as well as the west walls of the depletion. The increased S4 values at the depletion walls are most likely to be caused by the larger background electron density at the walls as opposed to the lower electron density in the interior of the depletion. An interpretation of the above observation along with the observed propagation direction (eastward) in Figs. 4 and 5 suggests that the possible source of the observed irregularities is an extension of the equatorial plasma bubbles.

In order to better understand the presence of electron density irregularities, Fig. 8 shows the temporal variations in the ROTI values, estimated from the three receivers listed in Table 1, during 16:00–24:00 UT on June 11 (top), June 12 (middle), and June 13 (bottom). The IPP latitudes in geomagnetic coordinates are shown in the color bar. The ROTI values have been estimated using data at a sampling
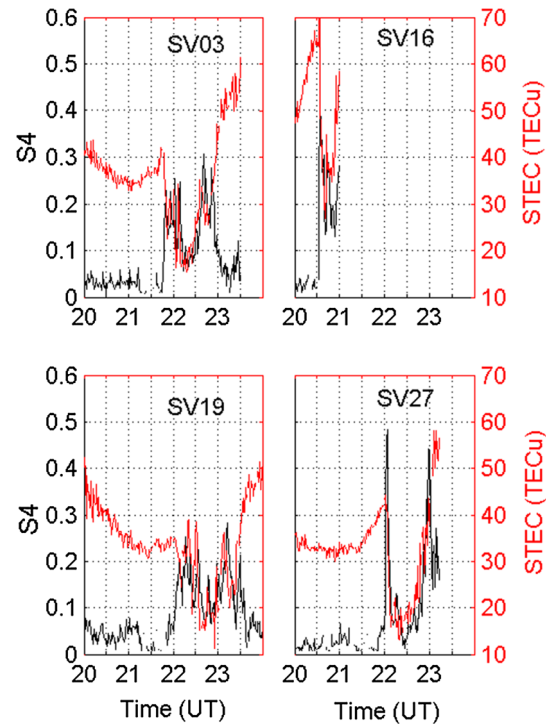

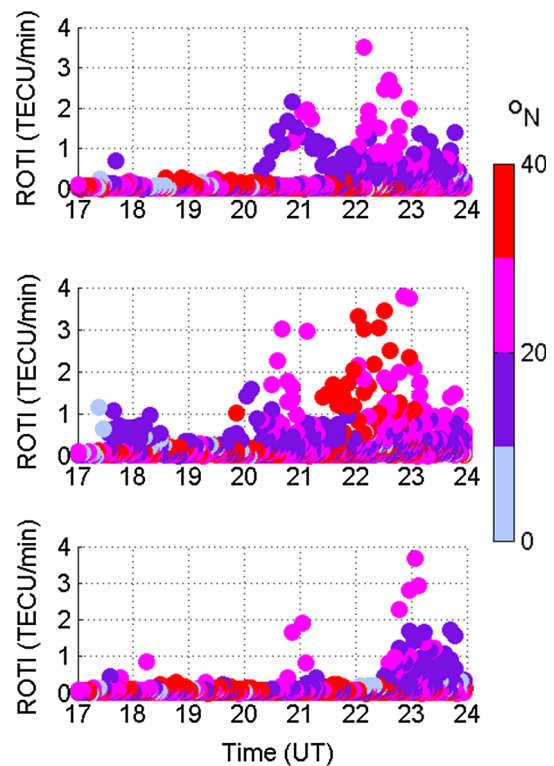**Fig. 7** Time variations in S4 (*black*) and STEC (*red*) along 4 different satellite-receiver links

Fig. 8 Temporal variations of ROTI on June 11 (*top*), 12 (*middle*) and 13 (*bottom*) of 2014. *Color bar* show the IPP geomagnetic latitudes in °N

rate of 30 s and hence ROTI values >0.5 TECU/min can only be used to indicate the presence of large-scale electron density irregularities with scale lengths of a few kilometers (Pi et al. 1997; Basu et al. 1999).

From Fig. 8, ROTI values greater than 0.5 TECU/min are observed during 17:30–18:30 UT on June 12 around 0–20°N geomagnetic latitudes, indicating the presence of large-scale irregularities near the anomaly crest. Such an enhancement in the ROTI values is not observed on June 11 or 13. This indicates that the background electrodynamic/neutral dynamic conditions on the night of June 12 were significantly different from those observed on the previous/next day. Similarly, enhanced ROTI with values greater than 1 TECU/min are observed during 20:00–23:00 UT around 20–40°N on June 12. ROTI values in the same range are observed on June 11 and 13; however, the maximum latitudinal extent of the observed irregularities is shorter, i.e., only around 10–30°N. An interesting feature to note from the figure is that on June 12, ROTI values even greater than 3 TECU/min are observed around 30–40°N during 22:00–23:00 UT, which coincides with the time when moderate L-band scintillation was recorded on SV27 (refer to Fig. 3). Thus, the presence of large-scale irregularities with a large latitudinal extension on the night of June 12 is confirmed from Fig. 8.

An interesting observation from Fig. 3 is that the presence of irregularities was first detected on SV16 at an IPP geographic latitude of about 32°N and geomagnetic latitude of about 25°N, corresponding to an apex height of about 1850 km at the geomagnetic equator. Simulations using the mean flux tube density model by Mendillo et al. (2005) have shown that density depletions associated with Equatorial Spread F (ESF) can easily reach altitudes above 2000 km in the equatorial plane. There have also been several observations showing that the ESF density depletions can reach very high altitudes, in some cases as high as 2500 km. However, these observations refer to times of strong geomagnetic storms, when the F-region plasma has been lifted considerably (Ma and Maruyama 2006; Huang et al. 2007). This is the first observation of an equatorial bubble reaching altitudes as high as 1850 km on a geomagnetically quiet day. As the upward velocities produced by the pre-reversal enhancement (PRE) over the equatorial latitudes during the summer months are smaller than those during the equinoxes, the probability of equatorial irregularities reaching apex heights of about 1850 km on a geomagnetically quiet day during the month of June is very low.

The irregularities observed over the midlatitude station of Nicosia are connected through the magnetic field lines to around 1850 km over the geomagnetic equator in the African longitude sector. Limited studies have been carried out in this sector as compared to the Asian/South American sector. Paznukhov et al. (2012) reported on the longitudinal, seasonal and local time occurrence of equatorial plasma bubbles and L-band scintillation over equatorial Africa during the solar minimum year of 2010. They have shown that over the East African longitude (about 40°E), shallower plasma bubbles are observed even during the summer solstice, a result that was consistent with the DMSP (Defense Meteorological Satellite Program) satellite observations reported in Gentile et al. (2006). Further to this, using ROCSAT-1 (Republic of China Satellite) data at 600 km, Su et al. (2006) have shown that the occurrence of topside equatorial plasma density irregularities over the African longitudinal sector is more prominent during the two equinoxes as well as the June solstice. Our observation of a plasma bubble reaching the midlatitudes is therefore quite consistent with these results.

The background ionospheric conditions on the night of June 12 are also investigated using the digisonde data from Nicosia and are presented in the next section.

Ionosonde measurements

It has been extensively reported in the literature that, at midlatitudes, scintillation occurrence is usually associated with the appearance of Range Spread F (RSF) on ionograms, which is identified as 'spread' in the F-region trace height due to irregular structures in electron density. Such irregular structures have been attributed to F-layer altitude modulation by large-scale atmospheric gravity waves (Bowman 1990) and to electrodynamic forces and large-scale plasma instabilities (Miller et al. 1997). The sequence of ionograms on June 11 and 12 recorded by the digisonde at Nicosia between 18:40 and 23:25 UT is shown in Figs. 9 and 10 respectively. The x axis is the frequency in MHz, and the y axis shows the virtual height in km.

The spread in the F-region trace, indicating the occurrence of RSF, during 22:10–23:25 UT on June 12 is very clear from Fig. 10. Such a spread in the F-region trace is not observed in Fig. 9, indicating the absence of RSF on June 11. It is well known that ionosonde observations are sensitive to electron density irregularities with scale sizes of the order of kilometers, so the gradual development of RSF on June 12, as observed on the ionograms, indicates the presence of irregularities of those scale sizes. The sequence of ionograms in Fig. 10 also shows a semi-transparent Es layer at 18:40 UT, when it can be observed at an altitude of 100 km. Between 19:50 and 22:10 UT, the Es layers have disappeared and range spread in the F-layer started to develop. On comparing Figs. 3 and 10, it can be observed that there is a difference in time when the L-band scintillation was first observed on SV16 at around 20:30 UT and when the RSF was observed on the ionograms, i.e., around 22:10 UT. This time difference is

Fig. 9 Sequence of ionograms recorded by the DPS-4D ionosonde on June 11, 2014, over Nicosia. The *x* axis is the frequency in MHz and the y axis shows the virtual height in km
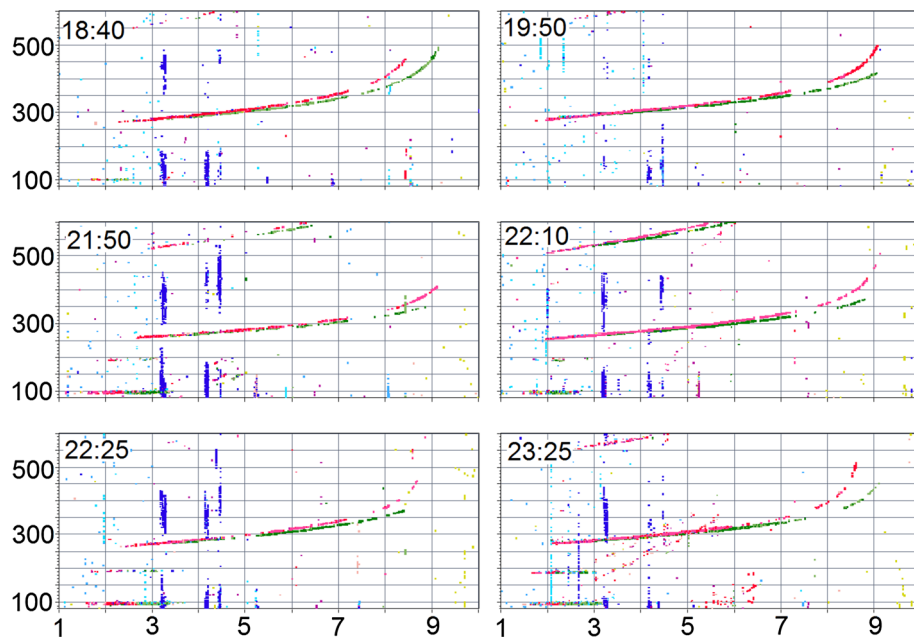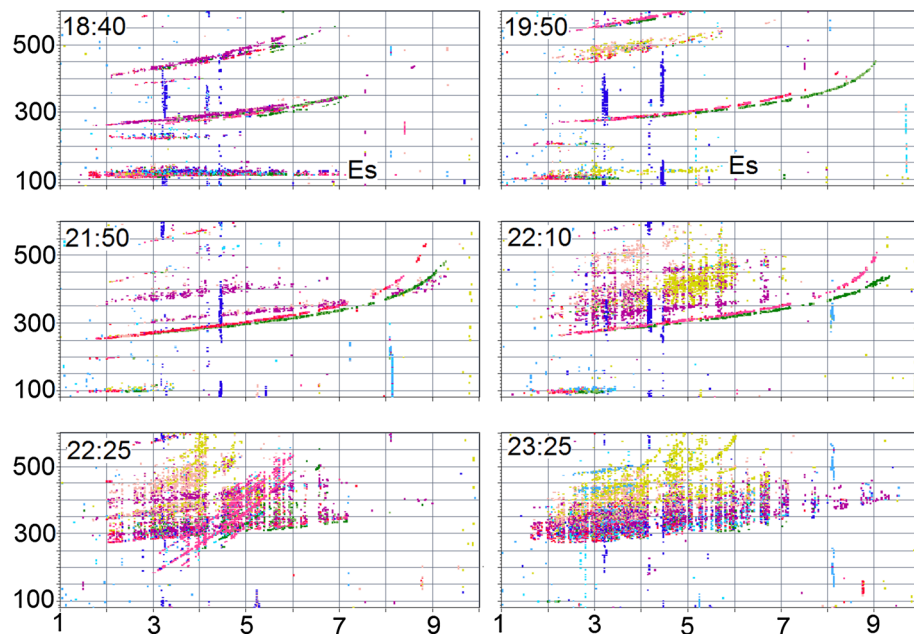

Fig. 10 Sequence of ionograms recorded by the DPS-4D ionosonde on June 12, 2014 over Nicosia. The *x* axis is the frequency in MHz and the *y* axis shows the virtual height in km

attributed to the fact that the GNSS receiver can monitor a wider ionospheric region as compared to the digisonde and therefore detects the presence of irregularities earlier. The digisonde detects the irregularities only after they have drifted to its field of view. Furthermore, a simultaneous occurrence of scintillation and RSF can be observed at about 22:10 UT, indicating the presence of hundred-meter- as well as kilometer-scale-size irregularities. This corroborates the earlier observation that these two scale size irregularities generally coexist, due to the fact that diffusion can induce an earlier decay of the smaller scale size irregularities (Rodrigues et al. 2004).

Figure 11 presents the variations in the F-region zonal drift velocity estimated from the digisonde during June 11–13, with positive values indicating eastward drifts. East–west drift velocities exceeding values of 40 m/s during 20:00–24:00 UT on June 12 can be clearly observed from this figure, indicating a strong eastward drift of the irregularities. Two distinct peaks in the drift velocity, with values of about 57 m/s at 19:48 UT and about 74 m/s at 22:22 UT, respectively, are observed. This is in agreement with the estimated velocity and propagation direction based on GNSS measurements as discussed earlier.
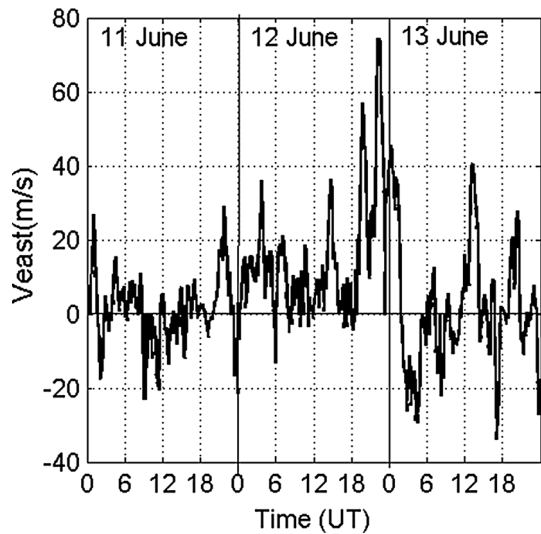
Fig. 11 East–west F-region drift velocities recorded over Nicosia during June 11–13, 2014
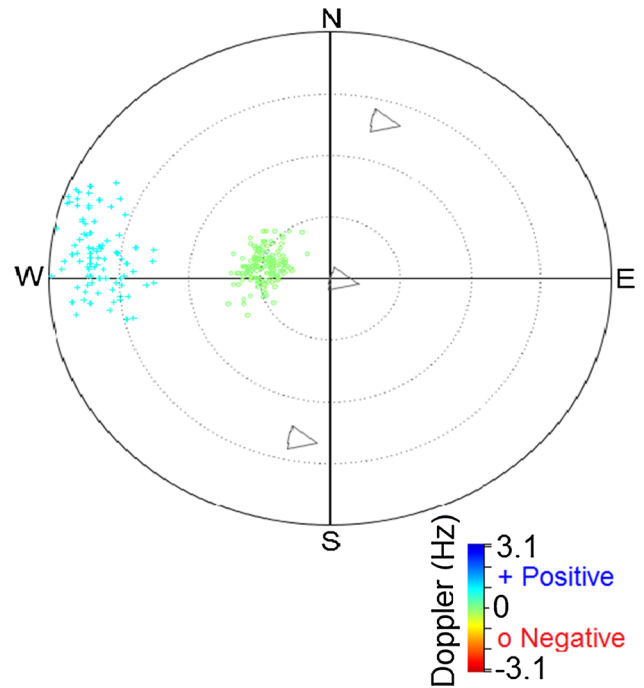

Fig. 13 Skymap over Nicosia on June 12, 2014, at 21:58 UT. The direction and size/shape of the *arrows* indicate that during this time, the resultant plasma motion was eastward with an increasing magnitude
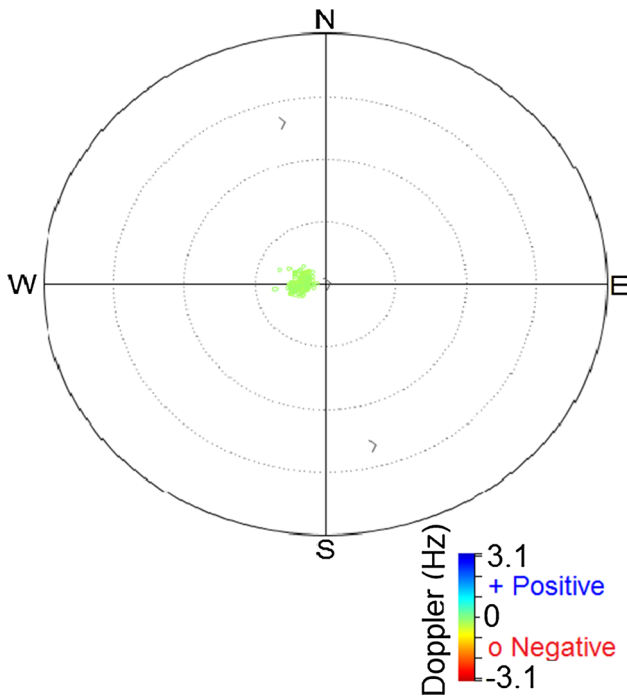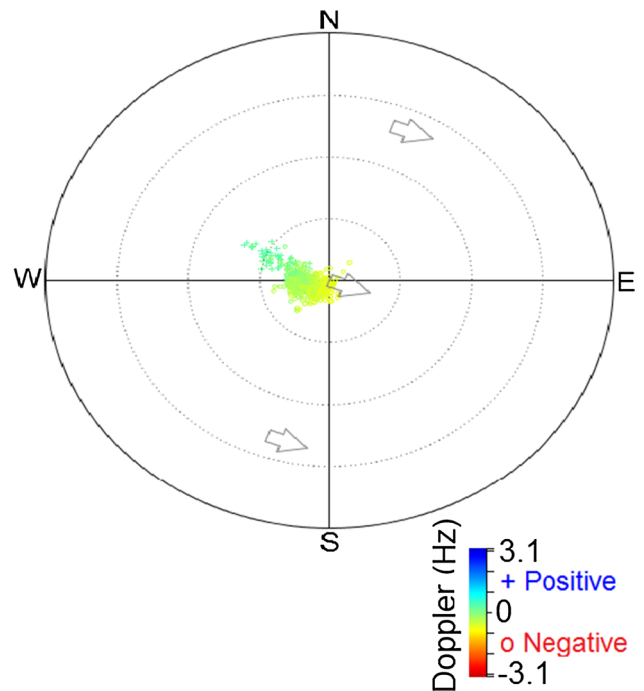

Fig. 12 Skymap over Nicosia on June 12, 2014, at 21:33 UT. The direction and size/shape of the *arrows* indicate that during this time, the resultant plasma motion was eastward with a small magnitude

Figures 12, 13 and 14 illustrate three skymaps on the night of June 12 displaying the reflection points in the F-region within a cone of 40° around the zenith and with concentric circles at 10° intervals. The color bar indicates the Doppler frequency in Hz and the '+' and 'o' symbols

Fig. 14 Skymap over Nicosia on June 12, 2014, at 22:13 UT. The direction and size/shape of the *arrows* indicate that during this time, the resultant plasma motion was eastward with a high value

Fig. 15 Digisonde HTI maps recorded over Nicosia during June 11–13, 2014
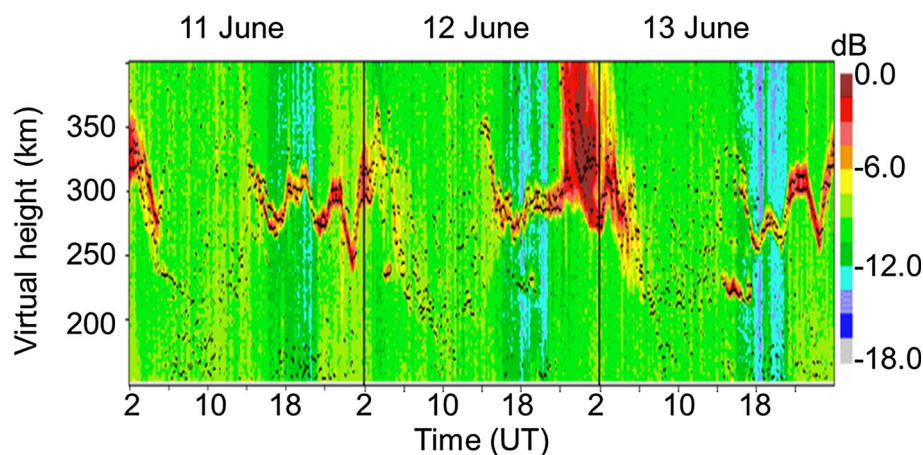
indicate positive and negative values of the frequency, respectively. The direction of the arrows in Figs. 12, 13 and 14 represents the dominant direction of the plasma motion in the horizontal plane, while the size and shape of the arrows is analogous to the magnitude of the plasma drift velocity. If the ionosphere is smooth and horizontally stratified, the skymaps will show a single source location at zero zenith angle. However, in the presence of horizontal gradients/tilts, the 'sources' will align along the direction of the gradient. The skymap at 21:33 UT, presented in Fig. 12, shows 'sources' with a negative Doppler frequency (o symbols) up to 10° zenith angle. The frequency and range span of these sources vary between 5.6–5.95 MHz and 317–330 km, respectively. The total number of sources was 205, and the center of the sources was about at zenith 3° and azimuth −87°. There is only a very small deviation from zero zenith angle, which indicates that during this time; the horizontal gradients/tilts in the ionosphere were very small.

The skymap at 21:58 UT, presented in Fig. 13, shows two sets of 'sources', one between 30° and 40° zenith angle with a positive Doppler (+ symbols) and the other between 5° and 15° zenith angle with a negative Doppler (o symbols). The total number of sources was 243, and the frequency and range span of these sources vary between 3.6–3.95 MHz and 280–305 km, respectively. During this time, the center of the 'sources' was about at zenith 18° and azimuth −82°. This deviation from zero zenith angle indicates the presence of horizontal gradients in the ionosphere, and the resultant azimuth of the 'sources' can be observed to be aligned along the east–west direction, which is typical of the magnetic field aligned irregularities.

The skymap at 22:13 UT, presented in Fig. 14, shows the situation after the RSF development. 'Sources' can be identified up to 10° zenith angle with both positive and negative Doppler (+ and o symbols). The frequency and

range span of these sources vary between 5.6–5.95 MHz and 317–330 km, respectively. The total number of sources was 663, and the center of the sources was about at zenith 3° and azimuth −102°. The resultant azimuth is still aligned along the east–west direction. Thus, the skymap at 21:58 UT, i.e., just before the onset of RSF, on the night of June 12 indicates the presence of magnetic field aligned irregularities, typically associated with equatorial plasma bubbles.

Figure 15 is a HTI plot during June 11–13, 2014 considering 5-min ionogram traces received within the frequency range 1.5–3.5 MHz with the color scale varying from strongest (red) to weakest (blue) signals. HTI maps show the intensity of the reflected signal as a function of time and altitude. The small black dots indicate points where the signal reflection strength maximizes. From Fig. 15, variations in the F-region height can be clearly observed during 02:00–06:00 UT and during 14:00–24:00 UT. On June 11 and 13, the F-region height variations are smooth and the reflected signal is from virtual heights close to 300–350 km. During 22:00–24:00 UT on June 12, the HTI map is spread over a large F-region altitude range and the reflected signal intensity is greater than -1.5 dB, clearly showing the development of RSF. This large altitudinal spread in the HTI map is due to multiple reflections between the F2 layer peak and the ground, as the signal is very strong and indicates the presence of irregularities. A remarkable characteristic identified around this time is the periodic descend of reflections (as represented by the black dots) between 400 and 300 km. This feature can be attributed to off-angle reflections from electron density depletions and can be interpreted as an approaching ionospheric instability which caused the ionospheric F2 region to break up into spread F (Lynn et al. 2011).

The results presented above indicate that under suitable background ionospheric conditions, equatorial plasma

bubbles can map to very high altitudes and cause moderate amplitude L-band scintillation over the midlatitudes even during periods of quiet geomagnetic activity.

Conclusions

An insight on the observations of moderate GPS L1 amplitude scintillation over the midlatitude station of Nicosia, Cyprus, on a geomagnetically quiet day is presented. The scintillation data were recorded by a Septentrio PolaRxS GNSS scintillation monitor receiver. The high S4 values observed on the night of June 12, 2014, were found to correspond with large variations in ROT, indicating the presence of steep electron density gradients. The STEC and S4 variations indicate the presence of electron density depletions accompanying scintillation occurrence. The apparent horizontal drift velocity and propagation direction of the irregularities were estimated as about 49 m/s and eastward, respectively, value and feature consistent with those of equatorial plasma bubbles. An interpretation of the above observation is that the possible source of the irregularities causing L-band scintillation is an extension of the equatorial plasma bubbles to apex heights of about 1850 km over the magnetic equator. The occurrence of scintillation was associated with the appearance of RSF on the ionograms recorded at Nicosia. The HTI plot and the skymaps generated using the ionogram data showed the presence of electron density depletions. The overall conclusion is that the midlatitude ionosphere may be more active than previously thought and that further studies on the implications of equatorial and low latitude ionospheric behavior are necessary. This is particularly relevant for the GNSS user community and related applications.

References

Alfonsi L, Spogli L, De Franceschi G, Romano V, Aquino M, Dodson A, Mitchell CN (2011) Bipolar climatology of GPS ionospheric scintillation at solar minimum. Radio Sci. doi:10.1029/2010RS004571

Aquino M, Moore T, Dodson A, Waugh S, Souter J, Rodrigues FS (2005) Implications of ionospheric scintillation for GNSS users in Northern Europe. J Navig. doi:10.1017/S0373463305003218

Basu S, Groves KM, Quinn J, Doherty P (1999) A comparison of TEC fluctuations and scintillations at Ascension Island. J Atmos Sol Terr Phys. doi:10.1016/S1364-6826(99)00052-8

Basu S, Groves KM, Basu Su, Sultan PJ (2002) Specification and forecasting of scintillations in communication/navigation links: current status and future plans. J Atmos Solar-Terr Phys 64:1745–1754

Bowmen GG (1990) A review of some recent work on midlatitude spread-F occurrence as detected by ionosondes. J Geomagn Geo Electr 2:109–138

Bust GS, Gaussiran TL II, Coco DS (1997) Ionospheric observations of the November 1993 storm. J Geophys Res 102(7):14293–14304

Carter BA, Zhang K, Norman R, Kumar VV, Kumar S (2013) On the occurrence of equatorial F-region irregularities during solar minimum using radio occultation measurements. J Geophys Res Space Phys. doi:10.1002/jgra.50089

Ciraolo L, Spalla P (1997) Comparison of ionospheric total electron content from the Navy Navigation Satellite system and the GPS. Radio Sci 32:1071–1080

Fujita M, Sinno K, Ogawa T (1982) Frequency dependence of ionospheric scintillations and its application to spectral estimation of electron density irregularities. J Atmos Terr Phys 44:13–18

Gentile LC, Burke WJ, Rich FJ (2006) A global climatology for equatorial plasma bubbles in the topside ionosphere. Ann Geophys. doi:10.5194/angeo-24-163-2006

Hajkowicz LA (1994) Types of ionospheric scintillations in southern midlatitudes during the last sunspot maximum. J Atmos Terr Phys 56:391–399

Hajkowicz LA, Minakoshi H (2003) Midlatitude ionospheric scintillation anomaly in the Far East. Ann Geophys 21:577–581

Haldoupis C, Meek C, Christakis N, Pancheva D, Bourdillon A (2006) Ionogram height-time intensity observations of descending sporadic E layers at midlatitude. J Atmos Solar-Terr Phys 68:539. doi:10.1016/j.jastp.2005.03.020

Huang CS, Foster JC, Sahai Y (2007) Significant depletions of the ionospheric plasma density at middle latitudes: a possible signature of equatorial spread F bubbles near the plasmapause. J Geophys Res 112:A05315. doi:10.1029/2007JA012307

Ji S, Chen W, Weng D, Wang Z (2015) Characteristics of equatorial plasma bubble zonal drift velocity and tilt based on Hong Kong GPS CORS network: from 2001 to 2012. J Geophys Res Space Phys. doi:10.1002/2015JA021493-T

Kersley L, Aarons J, Klobuchar JA (1980) Nighttime enhancements in total electron content near Arecibo and their association with VHF scintillation. J Geophys Res 85:4214–4222

Kintner PM, Kil H, Beach TL, de Paula ER (2001) Fading timescales associated with GPS signals and potential consequences. Radio Sci 36:731–743. doi:10.1029/1999RS002310

Ledvina BM, Makela JJ, Kintner PM (2002) First observation of intense GPS L1 amplitude scintillations at midlatitude. Geophys Res Lett. doi:10.1029/2002GL014770

Ledvina BM, Kintner PM, de Paula ER (2004) Understanding spaced-receiver zonal velocity estimation. J Geophys Res 109:A10306. doi:10.1029/2004JA010489

Lynn KJW, Otsuka Y, Shiokawa K (2011) Simultaneous observations at Darwin of equatorial bubbles by ionosonde-based range/time displays and airglow imaging. Geophys Res Lett 38:L230101. doi:10.1029/2011GL049856

Lynn KJW, Otsuka Y, Shiokawa K (2013) Ionogram-based range-time displays for observing relationships between ionosonde satellite traces, spread F and drifting optical plasma depletions. J Atmos Sol-Terr Phys 98:105–112

Ma G, Maruyama T (2006) A super bubble detected by dense GPS network at east Asian longitudes. Geophys Res Lett 33:L21103. doi:10.1029/2006GL027512

Maruyama T (1990) ExB instability in the F-region at low to midlatitudes. Planet Space Sci 38:273–285

Mendillo M, Zesta E, Shodhan S, Sultan PJ, Doe R, Sahai Y, Baumgardner J (2005) Observations and modeling of the coupled latitude-altitude patterns of equatorial plasma depletions. J Geophys Res 110:A09303. doi:10.1029/2005JA011157

Miller CA, Swartz WE, Kelley MC, Mendillo M, Nottingham D, Scali J, Reinisch B (1997) Electrodynamics of midlatitude spread F 1. Observations of unstable, gravity wave-induced ionospheric electric fields at tropical latitudes. J Geophys Res 102:11521–11532

Ogawa T, Kumagai H (1985) Deep depletions of total electron content associated with severe midlatitude gigahertz scintillations during geomagnetic storms. J Geophys Res 90:6652–6656

Otsuka Y, Aramaki T, Ogawa T, Saito A (2006) A statistical study of ionospheric irregularities observed with a GPS network in Japan. Geophys Monogr Ser. doi:10.1029/167GM21

Paznukhov VV, Carrano CS, Doherty PH, Groves KM et al (2012) Equatorial plasma bubbles and L-band scintillations in Africa during solar minimum. Ann Geophys. doi:10.5194/angeo-30-675-2012

Perkins FW (1973) Spread F and ionospheric currents. J Geophys Res 78:218–226

Pi X, Mannucci AJ, Lindqwister UJ, Ho CM (1997) Monitoring of global ionospheric irregularities using the worldwide GPS network. Geophys Res Lett 24:2283–2286

Prölss GW (1993) Common origin of positive ionospheric storms at middle latitudes and the geomagnetic activity effect at low latitudes. J Geophys Res 98:5981–5991. doi:10.1029/92JA02777

Reinisch BW, Scali JL, Haines DM (1998) Ionospheric drift measurements with ionosondes. Ann Geofis 41:695–702

Reinisch BW, Huang X, Galkin IA, Paznukhov V, Kozlov A (2005) Recent advances in real-time analysis of ionograms and ionospheric drift measurements with digisondes. J Atmos Solar-Terr Phys 67:1054–1062

Rodrigues FS, de Paula ER, Abdu MA, Jardim AC, Iyer KN, Kintner PM, Hysell DL (2004) Equatorial spread F irregularity characteristics over São Luıs, Brazil, using VHF radar and GPS scintillation techniques. Radio Sci 39:RS1S31. doi:10.1029/2002RS002826

Septentrio PolaRxS (2010) Septentrio PolaRxS application manual version 1.0.0

Su SY, Liu CH, Ho HH, Chao CK (2006) Distribution characteristics of topside ionospheric density irregularities: equatorial versus midlatitude region. J Geophys Res 111:A06305. doi:10.1029/2005JA011330

Tsugawa T, Kotake N, Otsuka Y, Saito A (2007) Medium-scale traveling ionospheric disturbances observed by GPS receiver network in Japan: a short review. GPS Solut 11(2):139–144. doi:10.1007/s10291-006-0045-5

Van Dierendonck AJ, Klobuchar J, Hua Q (1993) Ionospheric scintillation monitoring using commercial single frequency C/A code receivers. In: Proceedings of ION GPS 1993, Institute of Navigation, Salt Lake City, UT, Sept 1333–1342

Wautelet G, Warnant R (2014) Climatological study of ionospheric irregularities over the European midlatitude sector with GPS. J Geod 88:223–240. doi:10.1007/s00190-013-0678-4

Wautelet G, Warnant R (2015) Origin of high-frequency TEC disturbances observed by GPS over the European midlatitude region. J Atmos Solar-Terr Phys 133:67–78. doi:10.1016/j.jastp.2015.08.003

Sreeja Vadakke Veettil is a postdoctoral research fellow at the Nottingham Geospatial Institute of the University of Nottingham in the UK, involved in European Commission, European Space Agency and UK research council-funded projects. Her research focuses on assessing the effects of space weather on GNSS receivers and positioning errors aiming to improve the modeling of scintillation and to develop mitigation tools.

Haris Haralambous is an Assistant Professor in the Electrical Engineering Department at Frederick University, Cyprus, and head of the ionospheric research group. His research interests focus on ionospheric and space weather effects on radio systems as well as ionospheric morphology studies using ionosondes, GNSS and radio occultation techniques.

Marcio Aquino is an Associate Professor at the Nottingham Geospatial Institute of the University of Nottingham in the UK. He pioneered the deployment of ionospheric scintillation and TEC monitoring receivers in Northern Europe in 2001. His research has focused on ionospheric effects on GNSS, including system vulnerability to ionospheric disturbances and relevant countermeasures.